Spin waves and magnetic ordering in the quasi-one-dimensional $S=\frac{1}{2}$ antiferromagnet $BaCu_2Si_2O_7$

M. Kenzelmann,[1] A. Zheludev,[2] S. Raymond,[3] E. Ressouche,[4] T. Masuda,[5,6] P. Böni,[7] K. Kakurai,[8] I. Tsukada,[5,9] K. Uchinokura,[5,6] and R. Coldea[10,11]

[1]*Oxford Physics, Clarendon Laboratory, Oxford OX1 3PU, United Kingdom*

[2]*Physics Department, Brookhaven National Laboratory, Upton, New York 11973-5000*

[3]*CEA-Grenoble, DRFMC/SPSMS/MDN, 38054 Grenoble Cedex, France*

[4]*DRFMC/SPSMS/MDN, CENG, 17 rue des Martyrs, 38054 Grenoble Cedex, France*

[5]*Department of Applied Physics, The University of Tokyo, 6th Engineering Bldg., 7-3-1 Hongo, Bunkyo-ku, Tokyo 113-8656, Japan*

[6]*Department of Advanced Materials Science, The University of Tokyo, 6th Engineering Bldg., 7-3-1 Hongo, Bunkyo-ku, Tokyo 113-8656, Japan*

[7]*Laboratory for Neutron Scattering ETH & PSI, CH-5232, Villigen PSI, Switzerland*

[8]*Neutron Scattering Laboratory, Institute of Solid State Physics, The University of Tokyo, Tokai, Ibaraki 319-1106, Japan*

[9]*Central Research Institute of Electric Power Industry, 2-11-1, Iwato kita, Komae-shi, Tokyo 201-8511, Japan*

[10]*Oak Ridge National Laboratory, Solid State Division, Oak Ridge, Tennessee 37831*

[11]*ISIS Facility, Rutherford Appleton Laboratory, Oxon OX11 0QX, United Kingdom*

(Received 24 December 2000; revised manuscript received 17 April 2001; published 17 July 2001)

Elastic and inelastic neutron scattering were used to study the ordered phase of the quasi-one-dimensional spin-1/2 antiferromagnet $BaCu_2Si_2O_7$. The previously proposed model for the low-temperature magnetic structure was confirmed. Spin-wave dispersion along several reciprocal-space directions was measured and interchain, as well as in-chain exchange constants were determined. A small gap in the spin-wave spectrum was observed and attributed to magnetic anisotropy effects. The results are discussed in comparison with existing theories for weakly coupled quantum spin chain antiferromagnets.

DOI: 10.1103/PhysRevB.64.054422 PACS number(s): 75.25.+z, 75.10.Jm, 75.40.Gb

I. INTRODUCTION

The investigation of low-dimensional magnets has been a very active research field for the last two decades. First conceived as simple spin models, low-dimensional magnets revealed a far richer physical behavior than their more conventional three-dimensional (3D) counterparts, due to the importance of quantum fluctuations. Particularly interesting is the one-dimensional (1D) Heisenberg antiferromagnetic model (1D HAF), for which the Hamiltonian is written as

$$H = J \sum_{\mathrm{i}}^{\mathrm{chain}} \mathbf{S}_i \cdot \mathbf{S}_i + 1, \tag{1}$$

J being the exchange coupling constant. The ground state of the 1D $S=1/2$ HAF is a spin-singlet and can be characterized as ''marginal spin liquid'': while long-range order is absent, spatial spin correlations decay according to a power law, and thus represent quasi-long-range order.[1] The excitation spectrum is isotropic and gapless, and is described in terms of $S=1/2$ elementary excitations known as ''spinons.''[2] Physical excitations are composed of pairs of spinons, which gives rise to a two-spinon continuum.[3] This behavior is in stark contrast with that of 3D spin systems, that have long-range order in the ground state (''spin solid''), and where the spectrum is dominated by single-particle $S=1$ excitations (spin waves). The pure one-dimensional HAF is of course a physical abstraction since spin chains in real materials are always at least weakly coupled. To make a virtue of necessity, weakly coupled antiferromagnetic chains offer the opportunity to study the crossover from the quantum spin dynamics in a single chain to semiclassical spin waves in 3D systems.

$BaCu_2Si_2O_7$ was recently recognized as an almost ideal model system[4] for experimental investigation of this dimensional crossover. The silicate crystallizes in an orthorhombic crystal structure, space group *Pnma*, and the lattice constants are $a=8.862(2)$ Å, $b=13.178(1)$ Å, and $c=6.897(1)$ Å.[5] The Cu^{2+} spins are subject to a strong super-exchange interaction via the O^{2-} ions, producing weakly coupled antiferromagnetic chains that run along the crystallographic c axis.[6] Correspondingly, the magnetic susceptibility shows a broad maximum at around 150 K (Ref. 4) and its temperature dependence follows the theoretical Bonner-Fisher curve[7] with an intrachain coupling $J=24.1$ meV. The nearest-neighbor Cu-Cu distance within the chains is equal to $c/2$ (for a schematic view of the crystal structure see Fig. 1 in Tsukada *et al.*[4]). Weak interactions between the chains result in long-range antiferromagnetic ordering at $T_N=9.2$ K, as observed by bulk susceptibility and specific-heat measurements.[4] Preliminary neutron-diffraction studies provided an estimate for the ordered magnetic moment at low temperatures: $m_0=0.16\mu_B$.[4] In the ordered state the spins are aligned along the crystallographic c axis (chain axis). Early inelastic work suggested that the ratio of interchain to in-chain interactions J'/J in $BaCu_2Si_2O_7$ is intermediate compared to that in such well-known $S=1/2$ systems as $KCuF_3$ (a more 3D-like material) and Sr_2CuO_3 (an almost perfect 1D compound), as shown in Fig. 1.

In a recent short paper we reported studies of the interplay between single-particle and continuum dynamics in $BaCu_2Si_2O_7$.[8] We showed that at low frequencies the spectrum is dominated by resolution-limited spin waves and that the two-spinon continuum of a single chain is recovered

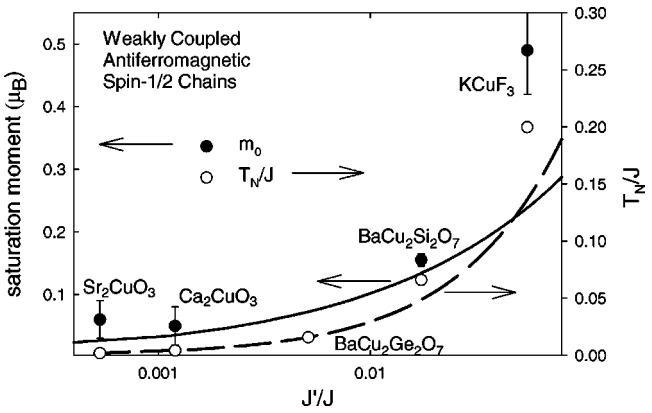

FIG. 1. The ordered moment and T_N/J for the known weakly coupled antiferromagnetic Heisenberg spin-1/2 chain compounds as a function of $|J'|/J$. For Sr_2CuO_3 (Ref. 10), Ca_2CuO_3 (Ref. 17), and $BaCu_2Ge_2O_7$ (Refs. 4 and 11), $|J'|$ was estimated using the predictions of the chain mean-field model (Ref. 15), while actual measured values were used for T_N. For $KCuF_3$ (Refs. 6 and 18) $|J'|$ was deduced from spin-wave bandwidth perpendicular to the chain axis. The lines are predictions of the chain mean-field model (Ref. 15).

above a threshold energy. For a better quantitative understanding of this behavior a detailed knowledge of both in-chain and interchain interactions in this system is required. The present paper is a detailed report on neutron-scattering characterization of this material. We focus on the 3D aspect, namely long-range magnetic order and spin-wave-like excitations. From measurements of the spin-wave dispersion along different reciprocal-space directions we determine all the relevant parameters of the system, such as the strengths and geometry of interchain coupling and magnetic anisotropy.

II. EXPERIMENT

Single crystals were grown using the floating-zone technique from a sintered polycrystalline rod. The crystals were carefully checked for twinning because the lattice constants along the *a* and *c* axis are very similar. The diffraction measurements were performed with a small sample with dimensions 3 mm^3 to exclude sizable extinction effects. The samples used in the inelastic scattering experiments were cylindrical in shape, 5 mm in diameter, and 50 mm in height. Up to three single crystals were co-aligned for the different experiments.

The neutron-scattering experiments were performed on five different instruments. The two-axis D23 diffractometer at the Institut Laue-Langevin (ILL), Grenoble, France, was used to investigate the ordered magnetic structure at low temperatures (setup I). D23 is a thermal neutron diffractometer with a lifting detector arm. The experiment was performed with a graphite monochromator at an incident energy $E_i = 14.7$ meV.

Spin-wave dispersion perpendicular to the chain axis was measured using two cold-neutron triple-axis spectrometers: the TASP spectrometer at Paul Scherrer Institut (PSI), Villigen, Switzerland (setup II), and the IN14 spectrometer at ILL (setup III). The zone-boundary energy was measured using the thermal neutron triple-axis spectrometer IN22 at ILL (setup IV). Preliminary measurements were also performed at the National Institute of Standards and Technology Center for Neutron Research (NCNR).

The experiment on TASP was performed with final neutron energy fixed at $E_f = 8$ meV. PG(002) reflections were used for monochromator and analyzer. The sample was mounted with its (h,h,l) and $(h,0,l)$ crystallographic plane in the horizontal scattering plane. The supermirror neutron guides gave a source-to-monochromator collimation of 70' both horizontally and vertically. The measurements in the $(h,0,l)$ plane were performed using 80'-80' collimators before and after the sample and distance collimation after the analyzer. For the measurements in the (h,h,l) plane, the use of 2-cm-wide slits cut the beam divergence before and after the sample down to effective values of 47'-60'. The energy resolution was 0.38 and 0.6 meV for the measurements in the (h,h,l) and $(h,0,l)$ crystallographic plane, respectively, as determined from the full width at half maximum (FWHM) of the quasielastic peak.

For the measurements using IN14 and IN22, PG(002) reflections were used for monochromator and analyzer. The sample was mounted with its $(0,k,l)$ crystallographic plane in the horizontal scattering plane. Final neutron energy was fixed at $E_f = 3$ meV and $E_f = 30.5$ meV, for the IN14 and IN22, respectively, with neutron guides defining the source-to-monochromator collimations of 30' and 60', respectively. 40'-40' collimators were used in both setups before and after the sample, and the use of slits cut the effective collimation of the IN22 setup down to 27'-40'. The energy resolution (FWHM) was 0.26 and 3.5 meV for the IN14 and IN22 measurements, respectively. Be or pyrolytic graphite filters were used after the sample to eliminate higher-order beam contamination.

The time-of-flight chopper spectrometer MARI at the ISIS Facility, Rutherford Appleton Laboratory, Oxon, United Kingdom, was used for the measurement of the magnetic excitations in a wide range of wave-vector transfers along the chain (setup V). The measurements were performed using a chopper-monochromated incident energy $E_i = 30$ meV allowing the measurement of the excitation spectrum up to 25 meV. The energy resolution was about 0.35 meV, as determined from the FWHM of the quasielastic peak. The resolution of the wave-vector transfer was given by the size of the sample, the detector, and their respective distance, and it was typically 0.05 reciprocal lattice units (r.l.u.) along the chain axis.

III. MAGNETIC STRUCTURE

To determine the spin structure in the ordered phase, 48 magnetic Bragg intensities were measured at $T = 1.5$ K using setup I. The main complication in the experiment was that all magnetic reflections appear on top of strong nuclear peaks. The following measurement procedure was implemented. For each reflection the nuclear intensity was measured in a rocking curve at $T = 10$ K $> T_N$. The peak intensity was then measured with high statistics both above and

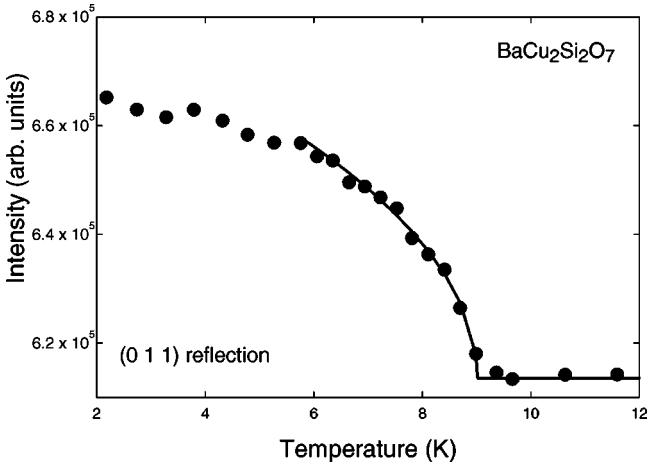

FIG. 2. Temperature dependence of the (0 1 1) reflection between 1.5 and 15 K. The scattering intensity above $T_N = 9.0$ K comes from the allowed nuclear Bragg reflection at (0 1 1). Below T_N, the intensity increases with decreasing temperature. The solid line is a fit to the data with the critical exponent $\beta = 0.25$ as explained in the text.

below T_N, and the difference was attributed to magnetic scattering. The integrated magnetic intensity was estimated from the measured intensity ratio and the integrated nuclear intensity. The magnetic structure was found to be totally consistent with that suggested in Tsukada *et al.*[4] The ordered moment at low temperature $m_0 = 0.15(3)\mu_B$ is parallel to the crystallographic *c* axis. Relative nearest-neighbor spin alignment is ferromagnetic along the *a* axis and antiferromagnetic along the *b* and *c* axes, respectively.

The temperature dependence of a few magnetic reflections was measured in the range $T = 1.5$–15 K as shown in Fig. 2 for the (0 1 1) peak. Below the ordering temperature T_N, the Bragg intensity increases with decreasing *T*. The measured peak intensity *I* is a sum of nuclear and magnetic contributions, the latter being proportional to the square of the sublattice magnetization *m*. The data were fit to a power-law form:

$$I(T) = I_0\left(\frac{T_N - T}{T_N}\right)^{2\beta} + N \quad \text{for} \quad T < T_N, \tag{2}$$

where I_0 is the magnetic intensity at $T = 0$ K, β is the order-parameter critical exponent, and *N* is the (nuclear) scattering intensity assumed to be *T* independent. A good fit is obtained with $\beta = 0.25(5)$ and $T_N = 9.0(0.05)$ K. The value of β is clearly below the critical exponent for a 3D antiferromagnet, and is in good agreement with the critical indexes measured in the quasi-1D materials $KCuF_3$ (Ref. 9) and Sr_2CuO_3.[10]

IV. DISPERSION OF MAGNETIC EXCITATIONS

A. Dispersion along [*h*,0,1] and [*h*,*h*,1]

Spin-wave dispersion at the 1D AF zone center $q_\parallel = \pi$ was measured along the [1,0,0] and [1,1,0] reciprocal-space directions at $T = 1.5$ K using setup II. Typical background-subtracted constant-*Q* scans are shown in Figs. 3 and 4. The

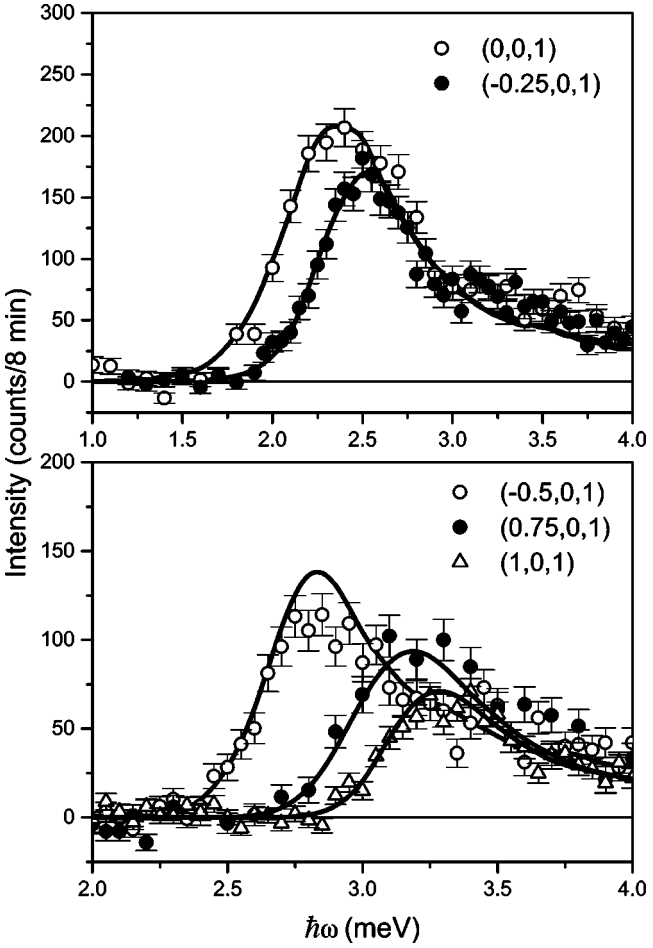

FIG. 3. Constant-*Q* scans measured at $T = 1.5$ K for three different wave-vector transfers on the [*h*,0,1] reciprocal-space rod (setup II). The background has been subtracted as described in the text. The solid lines represent global fits to the data using a model SMA cross-section function.

background was measured at $\mathbf{Q} = (h,0,1.25)$ $(h = 0-1)$ and $\mathbf{Q} = (h,h,1.25)$ $(h = 0-1)$, where no magnetic scattering is expected in the relevant energy transfer range, due to the steep dispersion along the chain axis. All measured scans show typical spin-wave peaks with a sharp onset on the low-energy side, and an extended high-energy resolution tail.

The data were analyzed using a model cross section written in the single-mode approximation (SMA), as will be discussed in detail in Sec. V. The cross section was numerically convoluted with the spectrometer resolution function, calculated in the Cooper-Nathans approximation.[12] Global fits to all data, as well as fits to individual scans, were performed in the energy transfer range 0–4.5 meV. As shown in Figs. 3 and 4, the model used gives an accurate description of the experimentally observed peak shapes. The transverse spin-wave dispersion relation deduced from the global fit is shown in Fig. 6 (solid lines), where symbols represent excitation energies obtained in fits to individual scans.

B. Dispersion along [0,*k*,1]

Dispersion along the [0,*k*,1] direction was measured using the high-resolution cold-neutron setup III at $T = 1.5$ K.

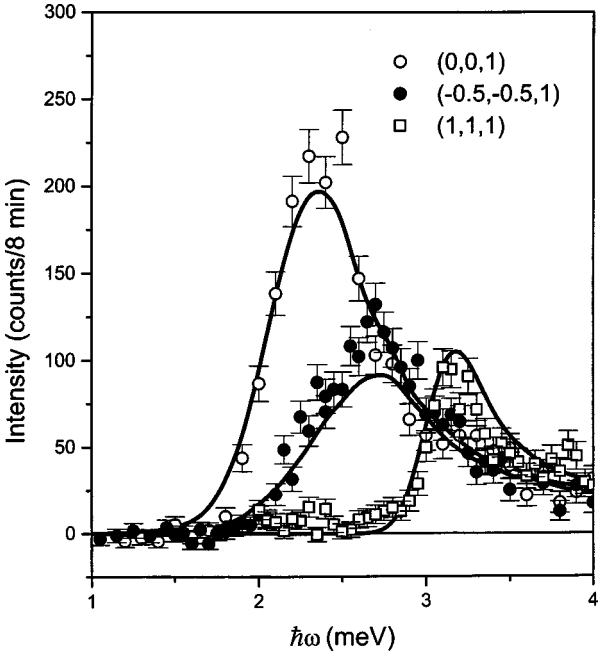

FIG. 4. Constant-Q scans collected at $T=1.5$ K for three different wave-vector transfers on the $[h,h,1]$ reciprocal-space rod (setup II). Background and lines as in Fig. 3.

Constant-Q scans were collected at wave vectors with k in the range $0 \leqslant k \leqslant 3$. Some of these data were presented elsewhere (see Fig. 2 in Ref. 8). Scans at the 3D AF zone centers $(0,1,1)$ and $(0,3,1)$ (Fig. 5) reveal the presence of a small gap in the spin-wave spectrum. In fact, there appear to be two separate modes with slightly different gap energies. These two branches correspond to different polarizations. The relative intensity of the lower-energy excitation at $\mathbf{Q}=(0,3,1)$ is clearly smaller than at $\mathbf{Q}=(0,1,1)$. Due to the intrinsic polarization dependence of the magnetic neutron cross section, the observed behavior is consistent with the higher-energy mode being polarized along the a axis of the crystal, and the lower-energy excitation polarized along b. This consideration is made quantitative by a global fit to all measured scans using an SMA cross section with built-in neutron polarization factors for the two branches (solid lines in Fig. 5).

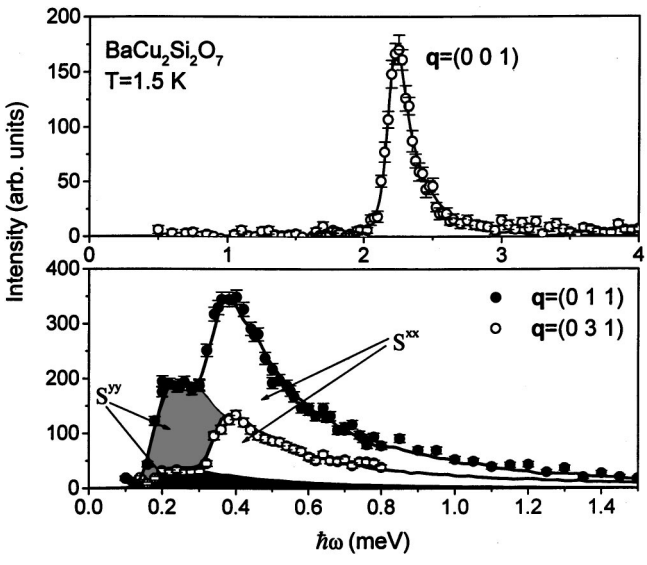

FIG. 5. Constant-Q scans collected at $T=1.5$ K for $\mathbf{Q}=(0,0,1)$, $\mathbf{Q}=(0,1,1)$, and $\mathbf{Q}=(0,3,1)$ (setup III). The solid line is a global fit to the data as described in the text. Shaded areas indicate partial contributions of two spin-wave branches with different polarization.

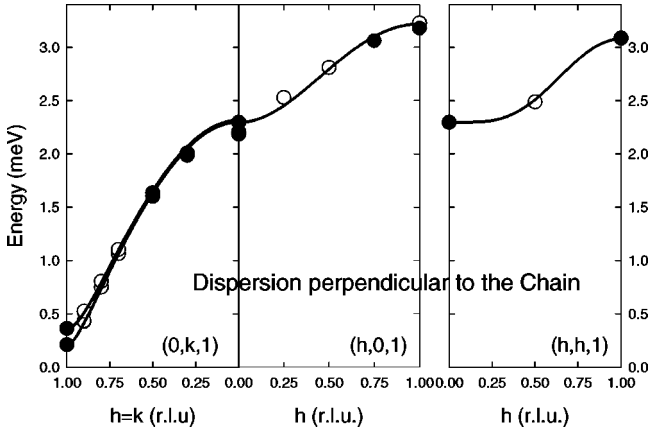

FIG. 6. Dispersion of the spin-wave excitations at $T=1.5$ K along three different crystallographic directions perpendicular to the chain axis. The open and closed circles show the excitation energies extracted from fits to individual scans. The open circle indicates that the measurements were actually performed at $(0,1-k,1)$, $(-h,0,1)$, and $(-h,-h,1)$, respectively. Error bars are smaller than the symbol size. The solid line is the dispersion determined in a global fit to the data using Eq. (7).

The spin-wave dispersion relation along the $[0,k,l]$ reciprocal-space direction is shown in Fig. 6 (solid lines). Here symbols represent fits to individual scans.

C. Dispersion along the chain axis

The dispersion of magnetic excitations along the chains was previously determined in constant-energy scans up to 16.5-meV energy transfer.[4] As part of the present work we performed additional measurements of this type using the time-of-flight technique (setup V). The incident neutron energy at the MARI spectrometer was set to 30 meV and the chain axis was aligned nearly perpendicular to the incoming beam direction. The scattered neutrons were counted by a large array of detectors, arranged in a half circle with radius 4 m vertically below the sample. The energy transfer was determined from the detection time. This allowed a simultaneous measurement of the neutron-scattering cross section on a two-dimensional surface in $(\mathbf{Q},\omega)$ space. The projection of the measurement surface onto the $(Q_\parallel,\omega)$ plane ($Q_\parallel$ being the wave-vector transfer along the chain axis) is shown in Fig. 7 for $T=8.5$ K. One clearly sees a ''fountain'' of magnetic scattering emanating from the $Q_\parallel=2\pi/c$ 1D AF zone center. We have previously demonstrated that in this energy range both spin waves and continuum contributions to the magnetic dynamic structure factor are important.[8] However, in the present experiment separating the two does not appear

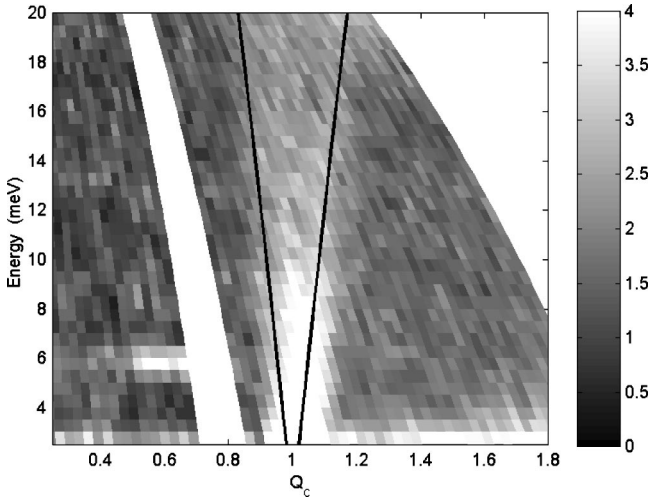

FIG. 7. Neutron-scattering intensity measured at 8.5 K using MARI as a function of wave-vector transfer along the chain axis and energy transfer. The color indicates the measured intensity according to the black and white color bar on the side. The empty spaces are due to the detector arrangement which is not continuous in the 2Θ scattering angle. The black line is the lower bound of the two spinon continuum for $J=24.1$ meV.

possible due to a poor wave vector resolution (typically 0.05 r.l.u. along the chains). The observed dispersion of magnetic excitations is consistent with the previous estimates of v_s. This is illustrated by the solid line in Fig. 7 that shows the calculated Des Cloizeaux–Pearson SMA dispersion relation for a 1D $S=1/2$ Heisenberg antiferromagnet,[13] or the lower bound of the two-spinon excitation continuum,[3] assuming $v_s=130.5$ meV Å.

D. Zone-boundary energy

To verify that only nearest-neighbor in-chain interactions are relevant, the measured value of v_s was compared to the excitation energy at the 1D AF zone boundary which corresponds to the sharp divergence on the lower bound of the two-spinon continuum, often refereed to as the De Cloizeaux–Pearson ''spin wave.''[13] The measurement was done at $T=1.5$ K in a constant-Q scan at the wave vector transfer $\mathbf{Q}=(0,0,2.5)$ $(Q_{\parallel}=5\pi/2)$, using setup IV (Fig. 8). The observed peak was analyzed using a Gaussian profile (solid line in Fig. 8) and the zone-boundary energy was determined: $\hbar\omega_{\mathrm{ZB}}=37.9(0.2)$ meV. With nearest-neighbor spin separation along the chain axis equal to $c/2$, for an $S=1/2$ 1D AF one expects $\hbar\omega_{\mathrm{ZB}}=\pi J/2$ and $v_s=\pi cJ/4$.[13] Assuming the nearest-neighbor model, for $BaCu_2Si_2O_7$ we thus obtain $J=24.1(1)$ meV and $v_s=130.5(5)$ meV Å, in excellent agreement with direct spin-wave velocity measurements and magnetic susceptibility data.[4]

V. DISCUSSION

Most measurements discussed in this paper have been performed below 4.5 meV, which is the threshold of the excitation continuum.[8,14] Below this energy, the spectrum is expected to be dominated by single-particle spin-wave excitations. The corresponding dynamic structure factor, and the spin-wave dispersion relation in particular, can be calculated using the chain mean-field (chain-MF) approximation.[15,16] As will be discussed below, this theoretical construct is in remarkably good quantitative agreement with our experimental results on $BaCu_2Si_2O_7$.

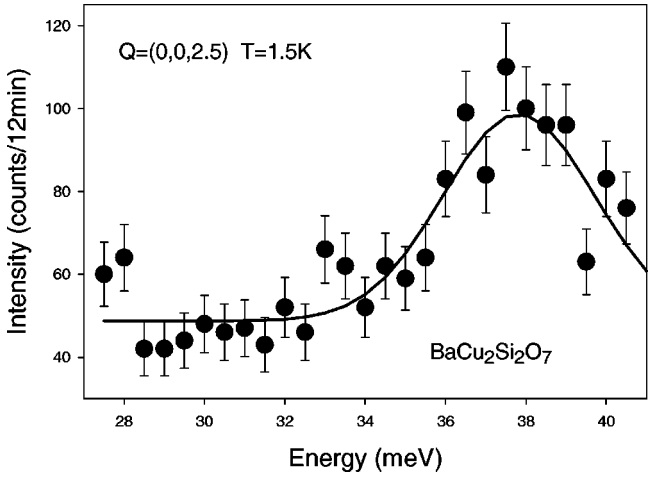

FIG. 8. Constant-Q scan collected at $T=1.5$ K at the 1D antiferromagnetic zone boundary $\mathbf{Q}=(0,0,2.5)$. The solid line is a Gaussian fit to the data.

A. Model Hamiltonian

We shall now describe the model Hamiltonian for $BaCu_2Si_2O_7$ that was used as a starting point in our data analysis. As mentioned above, a single nearest-neighbor Heisenberg exchange coupling constant J is sufficient to describe in-chain interactions. We found that in order to reproduce the observed dispersion in the perpendicular directions, three independent interchain exchange constants are required. The Cu^{2+} chains in $BaCu_2Si_2O_7$ form a rectangular lattice with nearest-neighbor Cu-Cu distances along the a and b axes of $a/2$ and $b/2$, respectively. We shall denote the corresponding exchange constants as J_x and J_y. In addition, we shall include exchange interactions along the [1,1,0] direction (third nearest-neighbor interchain Cu-Cu distance) in our model and label the corresponding coupling constant as J_3. The model Heisenberg Hamiltonian is then written as

$$H=\sum_i J\mathbf{S}_{\mathbf{r}_i}\mathbf{S}_{\mathbf{r}_i+\mathbf{c}/2}+J_x\mathbf{S}_{\mathbf{r}_i}\mathbf{S}_{\mathbf{r}_i+\mathbf{a}/2}+J_y\mathbf{S}_{\mathbf{r}_i}\mathbf{S}_{\mathbf{r}_i+\mathbf{b}/2}+J_3\mathbf{S}_{\mathbf{r}_i}\mathbf{S}_{\mathbf{r}_i+\mathbf{a}/2+\mathbf{b}/2}+J_3\mathbf{S}_{\mathbf{r}_i}\mathbf{S}_{\mathbf{r}_i+\mathbf{a}/2-\mathbf{b}/2}. \quad (3)$$

Here the sum is taken over all spins in the system and $\mathbf{r}_i$ is the position of spin i.

Following Schulz[15] and treating the interchain coupling in a mean-field treatment, the Hamiltonian transforms into an effective single-chain Hamiltonian which reads

$$H=\sum_i J\mathbf{S}_i\mathbf{S}_{i+1}-h\sum_i(-1)^i S_i^z-2NJ'm_0^2. \quad (4)$$

The magnetic moment is aligned along the z axis. Here N is the number of sites in the chain, $m_0=(-1)^i\langle S_i^z\rangle$ is the staggered magnetization, and $h=-4J'm_0$. The effective MF interchain coupling strength J' for this anisotropic coupling geometry is given by $J'\equiv\frac{1}{4}(2|J_x|+2|J_y|+4|J_3|)$.

B. Dynamic structure factor

Essler *et al.* have previously derived the SMA dynamic structure factor for weakly coupled $S=1/2$ antiferromagnetic chains in $KCuF_3$, using the chain-MF/random-phase approximation (chain-MF/RPA).[16] It is straightforward to adapt their result to the coupling geometry for the Hamiltonian given in Eq. (3):

$$S^{xx}(\mathbf{Q},\omega)\propto\frac{1}{\omega_x(\mathbf{Q})}\{\delta[\omega-\omega_x(Q)]-\delta[\omega+\omega_x(\mathbf{Q})]\}, \tag{5}$$

$$S^{yy}(\mathbf{Q},\omega)\propto\frac{1}{\omega_y(\mathbf{Q})}\{\delta[\omega-\omega_y(\mathbf{Q})]-\delta[\omega+\omega_y(\mathbf{Q})]\}, \tag{6}$$

$$\omega_{x,y}^2(\mathbf{Q})=\frac{\pi^2}{4}J^2\sin^2(\pi l)+\frac{\Delta^2}{J_y+2J_3-J_x}\times[J_y+2J_3-J_x+J(\mathbf{Q})]+D_{x,y}^2. \tag{7}$$

In this formula $S^{xx}(\mathbf{Q},\omega)$ and $S^{yy}(\mathbf{Q},\omega)$ are dynamic structure factors for excitations polarized along the a and b axes, respectively, and $\mathbf{Q}=(h,k,l)$ is the wave-vector transfer. Δ is the gap induced in the quantum spin chains by the effective staggered exchange field in the magnetically ordered state. This gap corresponds to the excitation energy at a point in reciprocal space where interchain interactions cancel out at the RPA level, e.g., $\Delta=\omega[\mathbf{Q}=(0.5,0.5,1)]$. $J(\mathbf{Q})$ is the Fourier transform of interchain coupling, and is given by

$$J(\mathbf{Q})=J_x\cos(\pi h)+J_y\cos(\pi k)+J_3\cos[\pi(h+k)]+J_3\cos[\pi(h-k)]. \tag{8}$$

Finally, the parameters D_x and D_y in Eq. (7) are anisotropy gaps for the two spin-wave branches, that we empirically include in the dispersion relation, as in Tsukada *et al.*[4]

The magnetic dynamic structure factor is related to the inelastic neutron-scattering cross section through the polarization factors and form factors for the magnetic ions involved:

$$\frac{d\sigma}{d\Omega dE'}\propto|f(Q)|^2[S^{xx}(\mathbf{Q},\omega)\sin^2(\hat{\mathbf{Q}},\hat{\boldsymbol{a}})+S^{yy}(\mathbf{Q},\omega)\sin^2(\hat{\mathbf{Q}},\hat{\boldsymbol{b}})]. \tag{9}$$

The model cross section defined by Eqs. (5)–(9) were numerically convoluted with the calculated spectrometer resolution function and used in global least-squares fits to the data for each experimental setting. The effective MF interchain coupling strength $|J'|\equiv\frac{1}{4}(2|J_x|+2|J_y|+4|J_3|)$ is related to the gap energy through $\Delta=6.175|J'|$.[15] The in-chain exchange constant was fixed at $J=24.1$ meV, while the parameters J_x, J_y, J_3, D_x, and D_y were refined. The following values were obtained: $J_x=-0.460(7)$ meV (ferromagnetic), $J_y=0.200(6)$ meV, $2J_3=0.152(7)$ meV, $D_x=0.36(2)$ meV, and $D_y=0.21(1)$ meV. This yields $\Delta=2.51$ meV and $|J'|=0.41$ meV. The obtained dispersion relation is shown in Fig. 6 in solid lines. Symbols indicate excitation energies obtained in fits to individual scans.

C. Comparison with the chains-MF model

The chain-MF theory does not only reproduce the observed dispersion relation, but is in fact in good quantitative agreement with the data. According to Schulz[15] the relations between m_0, T_N and $|J'|$ are given by

$$|J'|=\frac{T_N}{1.28\sqrt{\ln(5.8J/T_N)}}, \tag{10}$$

$$m_0=1.017\sqrt{|J'|/J}. \tag{11}$$

In our case, where $|J'|=0.41$ meV and $J=24.1$ meV, this gives $T_N=13$ K and $m_0=0.13$ μ_B. T_N is overestimated by the chain-MF theory due to quantum fluctuations not taken into account on the MF level. The remaining small difference between the ordered and estimated ordered moment can be attributed to the presence of a weak easy-axis (Ising-like) anisotropy which clearly should have the effect of enhancing long-range order at low temperatures. Indeed, this term, no matter how small, induces long-range order even in the purely 1D model at $T=0$ K.

VI. CONCLUSION

The obtained detailed characterization of $BaCu_2Si_2O_7$ provides a quantitative basis for the discussion of single-particle vs continuum excitations in weakly coupled spin chains in Zheludev *et al.*[8] The experimental data are remarkably well described by the quantum mean-field model.

ACKNOWLEDGMENTS

We would like to thank Dr. L. P. Regnault (CEA Grenoble) and Dr. A. Wildes for their assistance with experiments at ILL, Dr. S.-H. Lee for his assistance with preliminary measurements at NIST, Professor A. Tsvelik (Oxford University), Professor R. A. Cowley (Oxford University), and Dr. I. Zaliznyak (BNL) for illuminating discussions, and Mr. R. Rothe (BNL) for technical support. This work was supported in part by the U.S.-Japan Cooperative Program on Neutron Scattering, Grant-in-Aid for COE Research ''SCP coupled system'' of the Ministry of Education, Science, Sports, and Culture. Work at Brookhaven National Laboratory was carried out under Contract No. DE-AC02-98CH10886, Division of Material Science, U.S. Department of Energy. ORNL is managed for the U.S. D.O.E. by UT-Battelle, LLC, under Contract No. DE-AC05-00OR22725. One of the authors (M.K.) was supported by the Swiss National Science Foundation under Contract No. 83EU-053223.

[1] H. A. Bethe, Z. Phys. **71**, 205 (1931).
[2] L. D. Faddeev and L. A. Takhatajan, Phys. Lett. **85A**, 375 (1981).
[3] G. Müller, H. Thomas, H. Beck, and J. C. Bonner, Phys. Rev. B **24**, 1429 (1981).
[4] I. Tsukada, Y. Sasago, K. Uchinokura, A. Zheludev, S. Maslov, G. Shirane, K. Kakurai, and E. Ressouche, Phys. Rev. B **60**, 6601 (1999).
[5] J. A. S. Oliveira, Ph.D. thesis, Ruprecht-Karls-Universität, Heidelberg, 1993.
[6] S. K. Satija, J. D. Axe, G. Shirane, H. Yoshizawa, and K. Hirakawa, Phys. Rev. B **21**, 2001 (1980).
[7] J. C. Bonner and M. E. Fisher, Phys. Rev. **135**, A640 (1964).
[8] A. Zheludev, M. Kenzelmann, S. Raymond, E. Ressouche, T. Masuda, K. Kakurai, S. Maslov, I. Tsukada, K. Uchinokura, and A. Wildes, Phys. Rev. Lett. **85**, 4799 (2000).
[9] D. A. Tennant, S. E. Nagler, D. Welz, G. Shirane, and K. Yamada, Phys. Rev. B **52**, 13 381 (1995).
[10] K. M. Kojima, Y. Fudamoto, M. Larkin, G. M. Luke, J. Merrin, B. Nachumi, Y. J. Uemura, N. Motoyama, H. Eisaki, S. Uchida, K. Yamada, Y. Endoh, S. Hosoya, B. J. Sternlieb, and G. Shirane, Phys. Rev. Lett. **78**, 1787 (1997).
[11] I. Tsukada, J. Takeya, T. Masuda, and K. Uchinokura, Phys. Rev. B **62**, R6061 (2000).
[12] M. J. Cooper and R. Nathans, Acta Crystallogr. **23**, 357 (1967).
[13] J. des Cloizeaux and J. J. Pearson, Phys. Rev. **128**, 2131 (1962).
[14] A. Zheludev, M. Kenzelmann, S. Raymond, T. Masuda, K. Uchinokura, and S.-H. Lee, cond-mat/0105223 (unpublished).
[15] H. J. Schulz, Phys. Rev. Lett. **77**, 2790 (1996).
[16] F. H. L. Essler, A. M. Tsvelik, and G. Delfino, Phys. Rev. B **56**, 11 001 (1997).
[17] K. Yamada, J. Wada, S. Hosoya, Y. Endoh, S. Noguchi, S. Kawamata, and K. Okuda, Physica C **253**, 135 (1995).
[18] M. T. Hutchings, E. J. Samuelsen, G. Shirane, and K. Hirakawa, Phys. Rev. **188**, 919 (1969).